Bone Reports 20 (2024) 101738

Contents lists available at ScienceDirect

Bone Reports

journal homepage: www.elsevier.com/locate/bonr

Hyoid bone morphology in patients with isolated robin sequence – A case-control study utilizing 3D morphable models

C.P.O.M. Van Den Berg [a,1], K. El Ghoul [a,*,1], E. O'Sullivan [b], P.K. Guntaka [c], C.M. Resnick [c], B. Pullens [d], R.H. Khonsari [e], D.J. Dunaway [f], E.B. Wolvius [a], L.S. Van de Lande [a,e,f], M. J. Koudstaal [a,c,f]

[a] Department of Oral and Maxillofacial Surgery, Erasmus University Medical Center, Rotterdam, the Netherlands
[b] Department of Computing, Imperial College London, London, United Kingdom
[c] Department of Plastic and Oral Surgery, Boston Children's Hospital, Boston, United States of America
[d] Department of Otorhinolaryngology, Erasmus University Medical Center, Rotterdam, the Netherlands
[e] Service de Chirurgie Maxillofaciale et Chirurgie Plastique, Hôpital Necker - Enfants Malades, Assistance Publique - Hôpitaux de Paris, Faculté de Médecine, Université Paris Cité, Paris, France
[f] Craniofacial Unit, University College London, Great Ormond Street Hospital, London, United Kingdom

ARTICLE INFO

Keywords:
Hyoid bone
Robin sequence
Oropharyngeal impairment
Geometric morphometrics
Shape analysis

ABSTRACT

Background: Abnormalities of the hyoid bone are associated with impairment of oropharyngeal functions including feeding, swallowing, and breathing. Few studies have characterized anatomic abnormalities of the hyoid in patients with Robin sequence (RS), e.g. a less mineralized and voluminous hyoid. The purpose of this study was to compare normal hyoid bone morphology and hyoid bone morphology in children with isolated RS.
Methods: Three-dimensional (3D) reconstructions of the hyoid bone were obtained from CT-imaging of children with RS and unaffected controls. A 3D morphable model was constructed using Principal Component Analysis (PCA). Partial least squares – Discriminant Analysis (PLS-DA) and multivariate analysis of variance (MANOVA) were used to characterize and compare hyoid shape differences between patients with RS and an age-matched control group.
Results: The study included 23 subjects with RS (mean age 9.8 ± 10.3 months) and 46 age-matched control samples. A less voluminous hyoid was observed for the RS group with a larger lateral divergence of the greater horns compared to controls (MANOVA, p-value<0.001). The first shape variable from the PLS-DA model showed a significant correlation for the observed variance between the two groups (Spearman $R = -0.56$, p-value<0.001). The control samples and 151 CT-scans of subjects up to age 4 years were used to create a 3D morphable model of normal hyoid shape variation ($n = 197$, mean age 22.1 ± 13.1 months). For the normal 3D morphable model, a high degree of allometric shape variation was observed along the first principal component.
Conclusions: The 3D morphable models provide a comprehensive and quantitative description of variation in normal hyoid bone morphology, and allow detection of distinct differences between patients with isolated RS and controls.

1. Introduction

Robin Sequence (RS) is a rare congenital anomaly with a live birth incidence of approximately 11.6 per 100,000 newborns (Paes et al., 2015). RS is defined as the triad of micrognathia, glossoptosis and upper airway obstruction. In conjunction with micrognathia and glossoptosis, an abnormal positioning of the hyoid bone is also observed in patients with RS (Lee et al., 2016; Staudt et al., 2013). The hyoid bone is positioned more posteriorly and caudally contributing to decreased airway patency in children with RS compared to normal controls (Lee et al., 2016; Staudt et al., 2013). An association between respiratory distress and anomalies of the hyoid bone has been suggested in patients with RS (El Amm and Denny, 2008; Giudice et al., 2020).

Abnormalities of hyoid bone position are of particular importance in

* Corresponding author.
E-mail address: k.elghoul@erasmusmc.nl (K. El Ghoul).
[1] These authors contributed equally to this work.

https://doi.org/10.1016/j.bonr.2024.101738
Received 4 September 2023; Received in revised form 9 January 2024; Accepted 11 January 2024
Available online 13 January 2024

the pathogenesis of upper airway obstruction due to its central role in the aerodigestive tract. Mandibular distraction osteogenesis (MDO), an operation commonly used to relieve upper airway obstruction in infants with RS, has been shown to lead to both mandibular lengthening and anterior displacement of the hyoid (Li et al., 2022; Mahrous Mohamed et al., 2011). This advancement typically leads to an increase in airway patency and resolution of upper airway obstruction (Roy et al., 2009).

The hyoid bone is considered an unusual osseous structure in that is does not articulate with other bones. It is instead suspended by surrounding infra- and suprahyoid ligaments and musculature and plays a prominent role in oropharyngeal functions including feeding, swallowing, speech, and breathing. Abnormalities of the hyoid bone are associated with oropharyngeal impairment (AlJulaih and Menezes, 2023). Only few studies have reported on hyoid bone abnormalities in patients with RS. These studies showed differences in hyoid bone ossification on computed tomography (CT) scans in children with RS compared to the controls (El Amm and Denny, 2008; Giudice et al., 2020). The use of CT-scans allowed for a more comprehensive evaluation of hyoid bone abnormalities compared to two-dimensional radiographic imaging. However, the reported measures were analyzed using traditional measures, e.g. volume and distances.

Characterization of structural differences could improve our understanding of the hyoid bone's role in aerodigestive impairment in patients with RS. The purposes of this study are to: 1) compare hyoid bone morphology in children with isolated RS and a normal control group, and 2) describe normal hyoid bone morphology in children under 4 years-of-age. We hypothesized that the hyoid bone in patients with isolated RS is morphologically distinct from controls.

2. Material and methods

2.1. Study design and sample description

This was a retrospective case-control study of patients diagnosed with RS at the Boston Children's Hospital in Boston, Massachusetts, USA and the Erasmus Medical Center in Rotterdam, The Netherlands. Patients between 0 and 4 years with available CT-scans taken prior to any maxillofacial surgery were included. Patients with syndromic RS were excluded. A pre-existing dataset from Hôpital Necker – Enfants Malades, Paris, France of unaffected individuals between 0 and 4 years of age with maxillofacial CT-scans was used for the control group (Fig. 1) (E et al., 2021). This dataset consisted of CT-scans taken for a variety of indications including headache, epilepsy, or trauma assessment. Only scans of patients without structural abnormalities, i.e. brain and bone tumours, skull fractures, or craniofacial anomalies, were included. CT-scans of sufficient quality for 3D skeletal mesh construction and hyoid bone segmentation were included. Hyoid meshes with missing parts due to incomplete scanning were excluded. In case multiple scans eligible for inclusion were available for patients with RS, only one scan was included by the quality or age at time of the CT scan. This study received IRB approval at the Boston Children's Hospital (Protocol #P00023123) and the Erasmus Medical Center (MEC 2015-539).

2.1.1. Image processing

All CT-scans were obtained in DICOM format. The hyoid bone was segmented and converted to a three-dimensional (3D) triangular mesh object using semi-automated thresholding with a default bone setting in Mimics InPrint (Materialise, Leuven). The construction of a 3D morphable model requires meshes to have dense point-to-point correspondences, i.e. each mesh consisting of the same number of vertices connected in a consistent triangular pattern (E et al., 2022). A non-rigid iterative closest point (NICP) algorithm was used to achieve dense correspondence of included meshes after initial alignment in Wrap v3.4 (Russian3DScanner, Moscow) (Amberg et al., 2007). To aid the NICP registration process of hyoid meshes, an annotation template was defined with anatomic hyoid landmarks (Fig. 2). The template was used to rigidly align all hyoid samples through a partial Procrustes alignment by removing translation and rotation effects but preserving scale. The landmarks used in this study were derived from literature (Fakhry et al., 2013; Cotter et al., 2015; Pollard et al., 2011). Two additional semi-landmarks, landmarks 9 and 10, which represent the midpoint between landmarks 1–2 and 7–8 from a superior view, respectively, were defined for this study. These were used to avoid a rotational error of the lateral hyoid parts in the NICP registration process for the three parts individually following rigid alignment. The template mesh was created by symmetrizing and remeshing of a high-quality median aged mesh from the normal group dataset in MeshMixer (Autodesk, Toronto) and consisted of 2916 vertices and 5820 triangular faces (Fig. 2).

To assess annotation accuracy, two researchers (CvdB and KE) independently annotated 25 randomly selected hyoid meshes for inter-observer variability and annotation was repeated by CvdB after three months for intra-observer variability.

2.1.2. 3D morphable model

Principal Component Analysis (PCA) was used to construct a three-dimensional morphable model with the aligned registered meshes from the normal group (Alabort-i-Medina et al., 2014). In order to account for allometric shape variation, i.e. variation in shape as an effect of size, age is used as a surrogate marker for size. An age matched comparison for the RS group was made by randomly selecting control samples in a 3:1 ratio. As such, for each RS sample within an age group, three samples within the same age group were randomly selected as

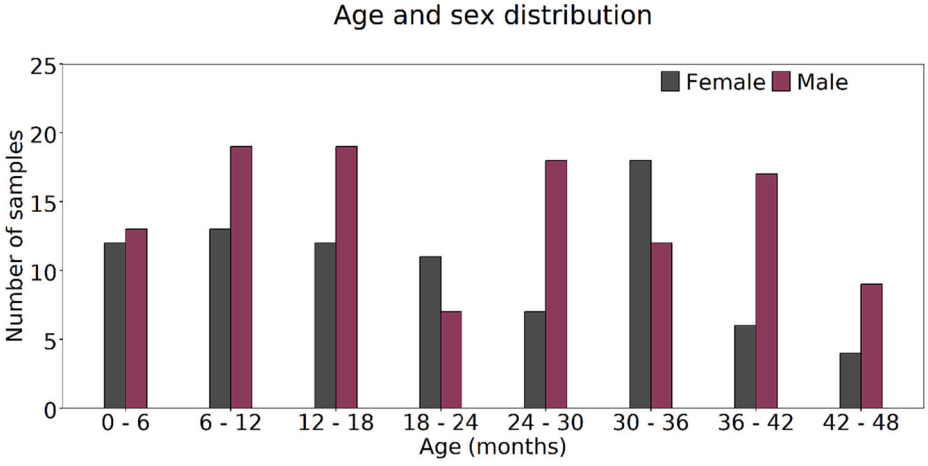

Fig. 1. A distribution of the ages and sex for the samples used to construct the 3D morphable model.

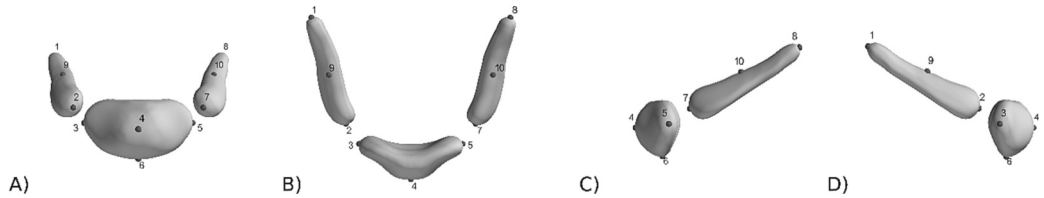

Fig. 2. Annotation template mesh of the hyoid with landmarks used for the 3D morphable model. The figure shows the **A**) frontal, **B**) superior, **C**) left lateral and **D**) and right lateral view.

controls from all samples used to construct the morphable model (Fig. 1). Due to a lack of control samples in the 1, 7 and 30 months age groups to meet the 3:1 ratio, synthetic control samples were generated from the 3D morphable model for these age groups using a multivariate Gaussian distribution (Fig. 3). The generated meshes were assessed against meshes in their respective age groups to represent realistic hyoid samples (Fig. 4). The model characteristics were evaluated with compactness, generalization and specificity, as described elsewhere, and reported in the supplemental figs. (E et al., 2021; E et al., 2022).

2.2. Statistical analysis

Descriptive statistics were calculated. Chi-square test was used to compare categorical variables and Student's *t*-test or non-parametric tests were used where applicable for continuous variables. To explore shape variation between the age-matched control group and RS samples, Partial least squares – Discriminant Analysis (PLS-DA) was used to extract shape variables most correlated with the direction of variance between groups. To assess whether hyoid shape in patients with RS was different from age-matched normal controls multivariate analysis of variance (MANOVA) was used on extracted shape variables. A leave-one-out cross-validation was used for assessment of classification of hyoid shapes with the PLS-DA model. The accuracy and F1-score are reported. The F1-score is obtained as the harmonic mean between sensitivity and the positive predictive value. With the 3:1 imbalance in control samples to RS samples this presents an adequate evaluation metric. Data analysis was conducted in Python v3.9. A p-value <0.05 was considered significant.

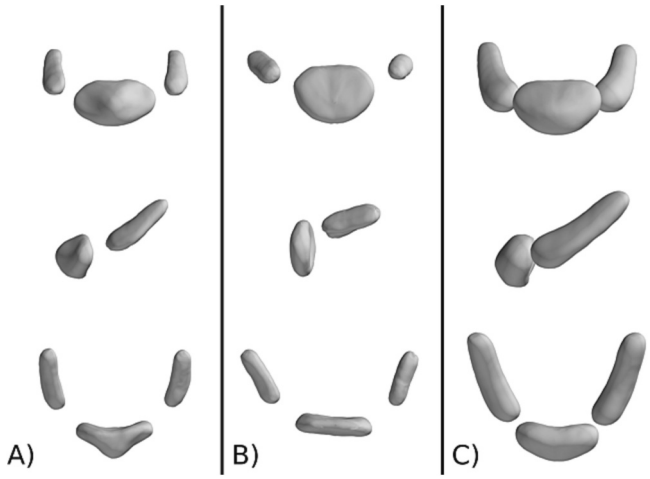

Fig. 4. A visualization of selected synthetic hyoid meshes in the control group at the age of **A**) 1 month, **B**) 7 months and **C**) 30 months. All generated meshes were considered realistic compared to the normal samples.

3. Results

3.1. Sample demographics

The RS group consisted of 23 samples (12, 52.2 % female) with a mean age of 9.8 ± 10.3 months (Supplemental Table 2). The control group consisted of 46 (22, 47.8 % female) samples. An additional 23 age-matched synthetic samples were generated from the hyoid morphable model to demonstrate normal anatomy for ages without matching samples (Fig. 3).

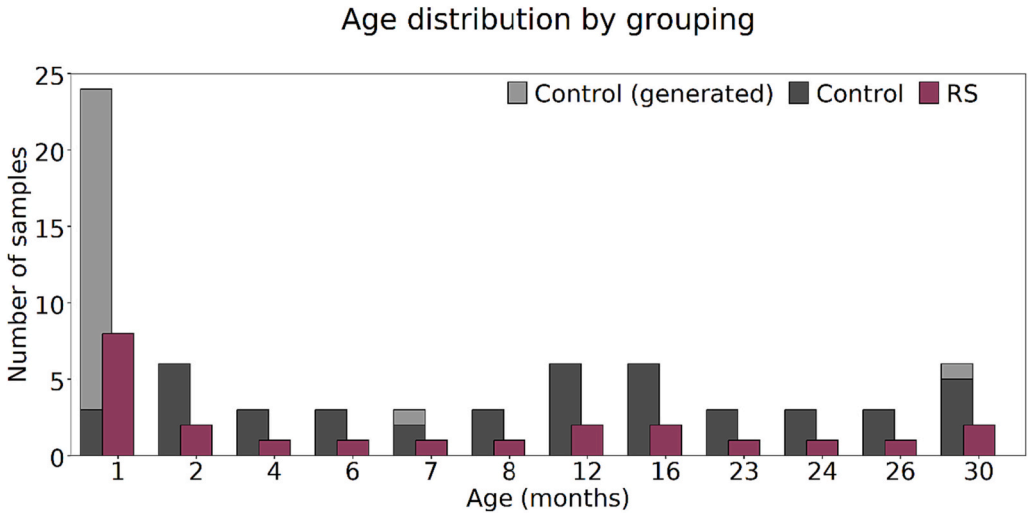

Fig. 3. Age distribution of the samples included for age-matched comparison. The control group consisted of hyoid samples from unaffected individuals (dark gray) and synthetic samples (light gray) generated from the 3D morphable model.

3.2. Landmark reliability

All landmarks showed Cartesian coordinate data with a Pearson correlation coefficient >0.90 for inter- and intra-class variability, indicating an excellent reliability and repeatability. In addition, the mean difference in absolute distance for all landmarks for both the inter- and intra-class variability was equal to or <1.0 mm.

3.3. 3D morphable model

PCA was used to construct a 3D morphable model of all normal hyoid meshes. The mean hyoid shape and shape variation along the first five principal components are shown in Fig. 5. The first principal component captured 62.3 % of variation and correlated well with age presenting allometric shape variation (Spearman's $R = 0.76$, p-value <0.001). Variation in hyoid morphology along successive principal components is primarily observed as a variation in relative angulation and size of the medial and lateral hyoid segments in varying dimensions (Fig. 5).

3.4. PLS-DA covariance between RS group and control group

PLS-DA analysis showed statistically significant correlations for seven of the first ten extracted shape variables and the observed variance between the RS group and the control group (Supplemental Table 3). Deformation of the mean hyoid along the first three shape variables is shown in Fig. 6. The first shape variable explains 25.3 % of variance between the two groups and denotes the highest correlation coefficient (Spearman's $R = -0.56$, p-value <0.001). This is associated with a smaller size of the individual hyoid bone parts for the RS group and a diverging angulation of the horns relative to the hyoid body. The second shape variable is not related to differences between the RS group and the control group with a low and non-significant correlation with the direction of variance between the two groups (Spearman's $R = -0.17$, p-value = 0.096). In contrast, this variable is associated with allometric shape variation with a high correlation coefficient for age (Spearman's $R = -0.80$, p-value <0.001). In addition, a majority (55.8 %) of variance is captured along this axis. For subsequent shape variables, the explained variance and correlation coefficients are smaller and are unlikely to present characteristic shape variation between the RS group and the control group (Supplemental Table 3).

Mean hyoid shapes for both groups are shown in Fig. 7. A less voluminous hyoid is observed for the RS group with a larger lateral

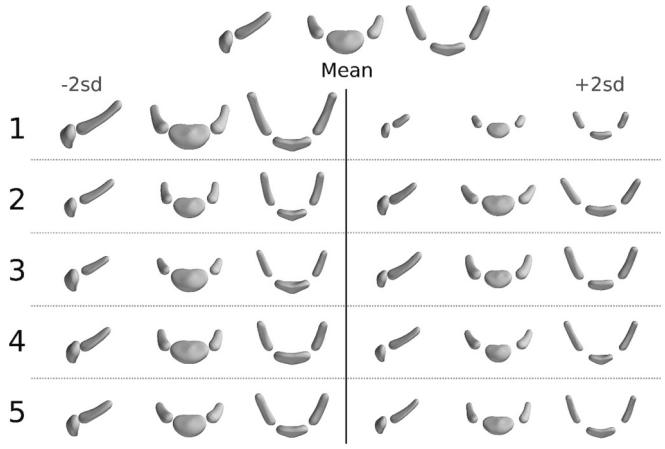

Fig. 5. Overview of the mean hyoid shape and the first five principal components of the normal hyoid morphable model. The top image shows a lateral, frontal, and superior view of the mean hyoid from left to right, respectively. The columns on the left and right correspond with hyoid instances ±2 standard deviations from the mean shape along the corresponding principal component (indicated by the number).

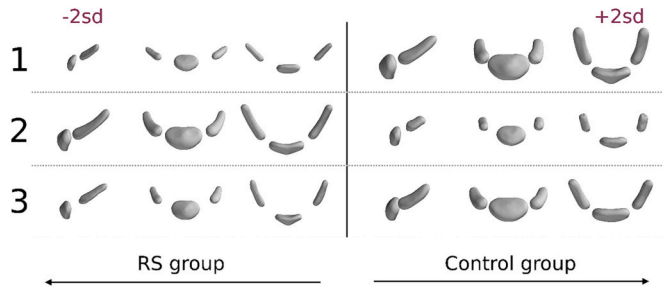

Fig. 6. Visualization of the hyoid shape deformations for the first three shape variables extracted from the PLS-DA model. The columns on the left and right correspond with ±2 standard deviations from the mean shape along the corresponding shape variable (indicated by the number) in a negative and positive direction, corresponding with the RS group and control group, respectively.

divergence of the greater horns. In a comparison of shape variables with MANOVA, a statistically significant difference was noted between the RS group and the control group (p-value <0.001). A biplot showing the separation between groups for the first two shape variables with a combined 81.1 % of explained variance is shown in Fig. 8A. The PLS-DA model showed an F1-score of 78.1 % and an accuracy of 90.2 % in distinguishing between the control group and RS group by hyoid shape in a leave-one-out cross validation (Fig. 8B). The observed separation in the biplot and an F1-score of 78.1 % indicate a good ability to distinguish between the RS group and control group by the PLS-DA hyoid shape variables, but also some degree of similarity. In addition, a larger spread is observed for the RS group than the control group in the biplot.

4. Discussion

The hyoid bone plays a central role in oropharyngeal functions, including maintaining airway patency, feeding and swallowing. These functions are typically impaired in children with RS. The hyoid bone is known to be positioned more posteriorly and caudally in children with RS contributing to limited airway patency. While its aberrant position and association with airway obstruction are well described, only few studies have reported on structural abnormalities of the hyoid bone in patients with RS (Lee et al., 2016; Staudt et al., 2013; Giudice et al., 2020). To consider its role in upper airway obstruction and oropharyngeal impairment in patients with RS, characterization of its unique structure is essential. Accordingly, the purposes of this study were to describe normal hyoid bone morphology and characterize variant morphology seen in patients with RS.

The results of this study suggest that the hyoid bone in patients with isolated RS is morphologically distinct from a normal, age-matched control group. The PLS-DA model was able to distinguish between the two groups with an accuracy of 90.2 % and F1-score of 78.1 % by hyoid shape differences. Roughly one fourth of variance in hyoid shape for the included age range could be attributed to differences between the two groups. In addition, both the normal PCA model and PLS-DA model suggest a high degree of allometric shape variation for the hyoid in patients with RS and unaffected patients.

Additionally, this study presents a 3D morphable model of the hyoid bone for children between 0 and 4 years of age. The 3D morphable model created in this study provides a comprehensive and quantitative description of variation in normal hyoid bone morphology for the included age range. From negative to positive extremes, the first principal component in the PCA model showcases an increasing prominence of the greater horns and hyoid body with a relative advancement of the greater horns towards the body and converging angulation. This may reflect progressive ossification of the hyoid bone and its constituents with age. The second principal component depicts a variation in the lateral extrusion of the greater horns and the third principal component shows a variation in the antero-posterior inclination of the hyoid body in

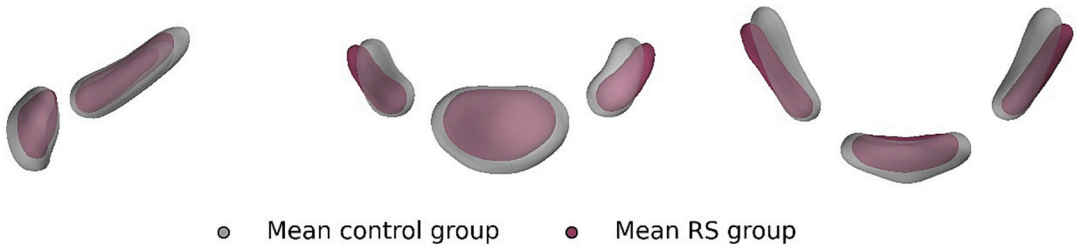

Fig. 7. The mean hyoid for the RS group (purple) and the control group (gray) from a lateral, frontal, and superior view. A less voluminous hyoid is observed for the RS group with a larger lateral divergence of the greater horns.

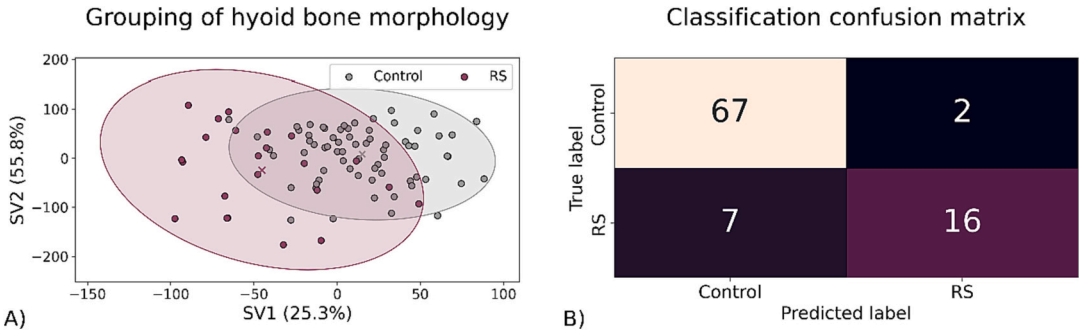

Fig. 8. **A**) Biplot for the first two shape variables (SV) extracted from the PLS-DA model showing a separation between the RS group and control group. The cross in the middle of the 95 % confidence ellipse indicates the mean for each group respectively. **B**) The classification confusion matrix for the PLS-DA model obtained from a leave-one-out cross validation. An associated F1-score of 78.1 % and accuracy of 90.2 % are obtained.

conjunction with the relative size of the greater horns. This morphable model can serve as a basis for future reference in characterization of hyoid bone morphology in other developmental conditions and forensic or anatomic studies. In addition, it allows for a comparative exploration of associations between hyoid bone abnormalities and functional impairment by providing a normal reference.

A visualization of morphological differences for the hyoid between the RS group and the control group was obtained from the PLS-DA model. In characterizing morphological differences, a relatively smaller and divergent hyoid was noted for the RS group. These unique characteristics may be reflective of posterior positioning related to mandibular micrognathia in children with RS. In addition, while the hyoid was morphologically distinct for the RS group compared to the control group, some degree of overlap was observed. In conjunction with the larger degree of variation in the RS group this could reflect a diverging range of hyoid bone abnormalities in line with the heterogeneous phenotype observed in patients with RS. This would be in line with reported differences in hyoid bone position and development in patients with isolated RS and syndromic RS (Lee et al., 2016; Giudice et al., 2020). These findings could form the starting point for exploring hyoid bone abnormalities and their association with functional oropharyngeal impairment in patients with RS.

Our findings are consistent with those presented by Giudice et al. who described hyoid bone abnormalities in patients with isolated and syndromic RS (Giudice et al., 2020). In their study, hyoid bone abnormalities were more common in patients with RS than the control group with a lower volume and lesser degree of hyoid bone ossification, particularly in those aged <4 months. In addition, the observed age associated changes in hyoid bone ossification and volume are concordant with the allometric component in hyoid bone morphology observed in this study. However, in their study a significant difference in age between the two samples was also noted with a significantly younger RS group. Considering allometric shape differences explaining a majority of variance in hyoid bone morphology this likely skewed their comparison. Our study characterizes differences in hyoid bone morphology between the two groups with an age-matched control. In addition, a comprehensive comparison utilizing quantitative statistical methods is used as opposed to a largely qualitative assessment. Furthermore, only one other study has reported on anatomical abnormalities of the hyoid bone in infants with RS (El Amm and Denny, 2008). This study qualitatively described hyoid bone abnormalities in a group of 28 patients with RS, including at least 9 with Stickler's syndrome. The hyoid bone abnormalities were categorized as normal, minor or severe and included partial or complete absence of the body or greater horns of the hyoid bone. Our study and the study by Giudice et al. identified similar findings both in subjects with RS and controls (Giudice et al., 2020).

As highlighted, future studies could leverage the comprehensive and quantitative description of hyoid bone morphology resulting from this study for various purposes. The association between hyoid bone abnormalities and functional impairment of feeding and breathing in RS could improve our understanding of their pathogenesis. Incorporation of additional parameters, e.g. hyoid bone position, mandibular deformity, treatment indications or syndromic diagnosis, can aid further characterization of the condition and tailoring management. In addition, the hyoid and its surrounding structures, e.g. stylohyoid muscle and ligament and posterior digastric muscle, are derived from the second and third pharyngeal arches whereas the mandible develops from the first pharyngeal arch. While micrognathia constitutes a cardinal feature in RS, identifying additional abnormalities such as those presented in the hyoid and their embryonic origin in relation to the mandible could provide a further understanding of the etiology in RS.

There are a number of limitations to this study. First, the dataset of RS meshes was relatively small, which may lead to selection bias. In addition, only those with CT-imaging could be included, which may introduce a bias towards more severely affected patients. To partly accommodate, in the age-matched comparison a ratio of controls to cases of 3:1 was chosen to allow for comparison of the RS sample against a range of shapes at a specific age. In addition, the sole inclusion of isolated RS cases further minimizes the risk of selection bias. Furthermore, a comparative analysis of shape variables utilizing PLS-DA is particularly well-suited for exploring shape differences between groups in case of a small sample size. Second, in addition to allometric

variation, various other factors may affect hyoid bone morphology e.g., body weight and height (Urbanova et al., 2013). These factors were not specifically accounted for in this study but assumed to be distributed evenly across the isolated RS cases and the controls. Furthermore, while only high-resolution CT-scans were used, it can be challenging to identify and adequately segment the hyoid bone for 3D reconstruction in light of continued ossification within the first few months of life.

In conclusion, this study showed distinct differences in hyoid bone morphology in patients with non-syndromic RS compared to an unaffected age-matched control group. In addition, the results show a significant allometric component for hyoid bone morphology for the included age range. The results of our study provide grounds for further study of hyoid bone abnormalities and their association with oropharyngeal impairment in patients with RS. The hyoid bone morphology seen in RS may pay a role in the respiratory distress seen in isolated RS patients, however future studies are needed to confirm this hypothesis. Moreover, further study is necessary to determine if differences in position and rotation of the hyoid bone in relation to the relevant surrounding structures play a role in the upper airway obstruction seen in RS.

Funding

The authors received no financial support for the research, authorship, and/or publication of this article.

Ethical approval

This study was approved by the Institutional Review Board of the Committee on Clinical Investigation at Boston Children's Hospital (Protocol #P00023123) and the Committee on Clinical Investigation at Erasmus Medical Center (MEC 2015-539).

Patient consent

Patient consent was not required.

CRediT authorship contribution statement

C.P.O.M. Van Den Berg: Writing – review & editing, Writing – original draft, Formal analysis, Data curation, Conceptualization. **K. El Ghoul:** Writing – review & editing, Writing – original draft, Visualization, Methodology, Formal analysis, Data curation, Conceptualization. **E. O'Sullivan:** Writing – review & editing, Visualization, Methodology, Formal analysis, Conceptualization. **P.K. Guntaka:** Methodology, Data curation. **C.M. Resnick:** Writing – review & editing, Writing – original draft, Methodology, Conceptualization. **B. Pullens:** Writing – review & editing, Writing – original draft, Methodology, Conceptualization. **R.H. Khonsari:** Writing – review & editing, Writing – original draft, Methodology, Conceptualization. **D.J. Dunaway:** Writing – review & editing, Conceptualization. **E.B. Wolvius:** Writing – review & editing, Writing – original draft, Supervision. **L.S. van de Lande:** Writing – review & editing, Writing – original draft, Methodology, Conceptualization. **M.J. Koudstaal:** Writing – review & editing, Supervision, Methodology, Conceptualization.

Declaration of competing interest

The authors declare no potential conflicts of interest with respect to the research, authorship, and/or publication of this article.

Data availability

Data will be made available on request.

Appendix A. Supplementary data

Supplementary data to this article can be found online at https://doi.org/10.1016/j.bonr.2024.101738.

References

Alabort-i-Medina J, Antonakos, E., Booth, J., Snape, P., Zafeiriou, S., 2014. Menpo: a comprehensive platform for parametric image alignment and visual deformable models. In: Proceedings of the 2014 ACM Conference on Multimedia (Mm' 14), pp. 679–682.

AlJulaih, G.H., Menezes, R.G., 2023. Anatomy, Head and Neck: Hyoid Bone. StatPearls, Treasure Island (FL).

Amberg, B., Romdhani, S., Vetter, T., 2007. Optimal step nonrigid ICP algorithms for surface registration. In: IEEE Conference on Computer Vision and Pattern Recognition, pp. 1–8.

Cotter, M.M., Whyms, B.J., Kelly, M.P., Doherty, B.M., Gentry, L.R., Bersu, E.T., et al., 2015. Hyoid bone development: an assessment of optimal CT scanner parameters and three-dimensional volume rendering techniques. Anat. Rec. (Hoboken) 298 (8), 1408–1415.

E, O.S., van de Lande, L.S., Oosting, A.C., Papaioannou, A., Jeelani, N.O., Koudstaal, M. J., et al., 2021. The 3D skull 0-4 years: a validated, generative, statistical shape model. Bone Rep. 15, 101154.

E, O.S., van de Lande, L.S., El Ghoul, K., Koudstaal, M.J., Schievano, S., Khonsari, R.H., et al., 2022. Growth patterns and shape development of the paediatric mandible - a 3D statistical model. Bone Rep. 16, 101528.

El Amm, C.A., Denny, A., 2008. Hyoid bone abnormalities in Pierre Robin patients. J. Craniofac. Surg. 19 (1), 259–263.

Fakhry, N., Puymerail, L., Michel, J., Santini, L., Lebreton-Chakour, C., Robert, D., et al., 2013. Analysis of hyoid bone using 3D geometric morphometrics: an anatomical study and discussion of potential clinical implications. Dysphagia 28 (3), 435–445.

Giudice, A., Belhous, K., Barone, S., Soupre, V., Morice, A., Vazquez, M.P., et al., 2020. The use of three-dimensional reconstructions of CT scans to evaluate anomalies of hyoid bone in Pierre Robin sequence: a retrospective study. J. Stomatol. Oral Maxillofac. Surg. 121 (4), 357–362.

Lee, V.S., Evans, K.N., Perez, F.A., Oron, A.P., Perkins, J.A., 2016. Upper airway computed tomography measures and receipt of tracheotomy in infants with Robin sequence. JAMA Otolaryngol. Head Neck Surg. 142 (8), 750–757.

Li, F., Li, H., Hao, J., Gao, Z., Wang, H., Chen, Y., 2022. Changes in hyoid bone position before and after distraction osteogenesis in infants with Robin sequence. J. Craniofac. Surg. 33 (4), 1051–1056.

Mahrous Mohamed, A., Al Bishri, A., Haroun, Mohamed A., 2011. Distraction osteogenesis as followed by CT scan in Pierre Robin sequence. J. Craniomaxillofac. Surg. 39 (6), 412–419.

Paes, E.C., van Nunen, D.P., Basart, H., Don Griot, J.P., van Hagen, J.M., van der Horst, C.M., et al., 2015. Birth prevalence of Robin sequence in the Netherlands from 2000-2010: a retrospective population-based study in a large Dutch cohort and review of the literature. Am. J. Med. Genet. A 167A (9), 1972–1982.

Pollard, J., Piercecchi-Marti, M.D., Thollon, L., Bartoli, C., Adalian, P., Becart-Robert, A., et al., 2011. Mechanisms of hyoid bone fracture after modelling: evaluation of anthropological criteria defining two relevant models. Forensic Sci. Int. 212 (1–3), 274 e1-5.

Roy, S., Munson, P.D., Zhao, L., Holinger, L.D., Patel, P.K., 2009. CT analysis after distraction osteogenesis in Pierre Robin sequence. Laryngoscope 119 (2), 380–386.

Staudt, C.B., Gnoinski, W.M., Peltomaki, T., 2013. Upper airway changes in Pierre Robin sequence from childhood to adulthood. Orthod. Craniofacial Res. 16 (4), 202–213.

Urbanova, P., Hejna, P., Zatopkova, L., Safr, M., 2013. The morphology of human hyoid bone in relation to sex, age and body proportions. Homo 64 (3), 190–204.